Spatial resolution enhancement/smoothing of stereo–particle-image-velocimetry data using proper-orthogonal-decomposition–based and Kriging interpolation methods

Hasan Gunes[a)]
Department of Mechanical Engineering, Istanbul Technical University, Gumussuyu, 34437 Istanbul, Turkey

Ulrich Rist[b)]
Institut für Aerodynamik und Gasdynamik, Universität Stuttgart, Pfaffenwaldring 21, D-70550 Stuttgart, Germany

(Received 25 July 2006; accepted 19 April 2007; published online 12 June 2007)

Methods for data reconstruction and spatial enhancement of experimental data for a transitional boundary layer with laminar separation bubble are investigated. Particularly, proper orthogonal decomposition (POD) is applied to direct numerical simulation (DNS) data to extract the DNS-based POD modes, which are projected onto the experimental data (via a least-squares procedure) in order to obtain model coefficients. These model coefficients are then used to reconstruct, "interpolate," and smooth the experimental data based on the DNS modes. In addition, in order to compare and assess the effectiveness of the present DNS-based procedure, Kriging interpolation is performed on the experimental (as well as numerical) data. These procedures are applied to time periodic (experimental) instantaneous spanwise vorticity (ω_z) at a constant spanwise location. We have demonstrated that particle-image-velocimetry (PIV)-based POD modes can be smoothed by Kriging interpolation, thus a noise-free reconstruction of PIV data can be achieved. It is also found that for very low resolution experimental data, DNS-based interpolation is superior over Kriging interpolation. On the other hand, Kriging interpolation based on the Gaussian correlation model works very well for sufficiently high resolution experimental data. The correlation parameter can be used to control the degree of smoothness in the data reconstruction. Both procedures effectively eliminate the unwanted noise in the experimental data. One important difference between the two procedures is that, with quite some confidence, the DNS-based procedure can also be used for "extrapolation" since the model coefficients do not depend on spatial variation. In fact, we show that near-wall spanwise vorticity, which is not available from experimental data, can be recovered faithfully. Moreover, the enhancement (interpolation and smoothing) of full *three*-dimensional PIV data has been performed by Kriging interpolation employing a Gaussian correlation model. © *2007 American Institute of Physics*.
[DOI: 10.1063/1.2740710]

I. INTRODUCTION

With the recent development of state-of-the-art quantitative data measurement techniques such as particle image velocimetry (PIV) and magnetic resonance imaging (MRI), experimentalists can now obtain flow (image) data with increasingly well resolved spatio-temporal accuracy, while ever expanding computational methods and hardware resources provide the computing community with even more highly resolved spatio-temporal numerical data compared to quantitative measurement techniques. When compared with the numerical data, an important feature of the experimental flow data is that it usually contains some undesired background noise and turbulence. In three-dimensional complex flows, structure extraction and vortex identification and tracking methods are of particular importance in order to visualize and understand the flow physics. In addition, many of the data visualization methods involve the evaluation of the gradients of the field variables, which further increase the noise level of the experimental data due to inevitable numerical differentiation errors. Therefore, utilization of various filtering as well as resolution enhancement techniques is usually required on the experimental data before employing any vortex identification method.[1]

In our recent paper,[2] we have analyzed proper orthogonal decomposition (POD) reconstruction of a transitional boundary layer flow with and without control and shown that POD modes extracted for a particular flow condition may be used to model the flow with modified conditions (through a control action, a change of Reynolds number, etc.) by modifying the temporal coefficients of the modes. While the cross projection approach (see Prabhu *et al.*[3]) is useful to evaluate the "suitability" of the nonoptimal POD modes (i.e., whether POD modes can be used for modified conditions), it has no practical use in the reconstruction of the unknown flow dynamics as it requires the complete flow field to be known *a*

[a)]Telephone: +90 212 293 1300. Fax: +90 212 245 0795. Electronic mail: guneshasa@itu.edu.tr
[b)]Telephone: +49 711 685 3432. Fax: +49 711 685 3438. Electronic mail: rist@iag.uni-stuttgart.de

priori. On the other hand, the least-squares method[2] offers a simple and effective approach to calculate the temporal coefficients, which we will use in this paper.

On the other hand, a recent new trend in simulation driven by experimental data has been presented by Sirisup *et al.*[4] and Ma *et al.*,[5] who extracted POD modes from (digital) PIV experiments and obtained an "experiment-based" POD simulation in an effort to implement a numerical algorithm in which simulation and experiment serve a "symbiotic feedback" system. In this way, experimental data are used to construct "realistic" simulation models to accurately predict the evolution of a given experimental state. In addition, the information extracted from the simulation may be used to enhance/improve the experimental results as well as to modify the experiment, e.g., to reorient the measurements to the proper location (see Refs. 4 and 5).

In this paper, we investigate the possibility of using DNS-based POD modes (i.e., POD modes extracted from DNS) in order to enhance (interpolate and smooth) the resolution of PIV data, a first step in realizing the integration of simulation and experiment for flow prediction. A least-squares fit of the low-resolution (and inherently noisy) PIV data on the DNS-based POD modes is performed in order to compute the temporal coefficients for the hybrid model. Then, these computed coefficients are used along with the high-resolution DNS-based POD modes in order to reconstruct the PIV data with the same *high resolution* as the DNS data. In addition, in order to assess the effectiveness of the present POD-based procedure, Kriging interpolation is also used to enhance the PIV data.

Kriging is an effective statistical estimation procedure that was named after D. G. Krige, a South African engineer who developed the procedure in order to predict mine ore ground water reserves more accurately from multipoint measurements. For the past several decades, Kriging has been used with success in geology and environmental engineering to interpolate the regionalized data (i.e., variables that fall between randomly scattered and completely deterministic data). It is assumed that the regionalized variable varies in a continuous form from one location to the next, and therefore points that are near each other have a certain degree of spatial correlation, but points that are widely separated are statistically independent.[6] Unlike other estimation procedures, Kriging provides a measure of the estimation error and associated confidence in the estimates.[7]

In ordinary Kriging, a model variogram, consisting of a set of mathematical functions that describe the spatial relationship, is constructed based on the known values. The appropriate model is chosen by matching the shape of the curve (i.e., polynomial, exponential, Gaussian, etc.) of the experimental variogram to the shape of the curve of the mathematical function (see Refs. 6 and 8). Based on the variogram used, optimal weights are assigned to known values in order to calculate the data at unknown points. The second approach in Kriging interpolation is based on the correlogram rather than the usual variogram (see Sacks *et al.*[9] for more information). It employs a polynomial regression routine that minimizes estimation variance from a predefined covariance model.

In the current paper, we adopt the Kriging interpolation based on the correlogram, implemented in the Matlab Toolbox DACE (Lophaven *et al.*[10]). Detailed information and aspects of the Matlab Toolbox DACE are given in Refs. 11 and 12. A brief overview of the method is also presented in Ref. 13. Given a sample of grid points and corresponding function values (design dataset), Kriging interpolation is based on a "surrogate model," which is obtained by the predetermined regression and correlation models. The correlation model usually contains a correlation parameter that defines implicitly the correlation length, which is optimized based on the variance estimate. Then, the constructed surrogate model is used to predict (interpolate) the function at unknown grid points. The regression model used in our study is based on second-order polynomials, and we employ a *Gaussian* correlation function as $R_i=\exp(-\theta_i d_i^2)$, where d_i is the distance and θ_i defines implicitly the correlation length. The Gaussian correlation function is suitable for continuously differentiable flow fields since it shows a parabolic behavior near the origin. It is also a suitable model function for *experimental* data, where usually some smoothing is necessary due to the background noise and/or measurement errors. Given a range of θ, an optimization procedure based on the variance estimate is performed in order to find the optimum value θ^*. In addition, if the flow field is anisotropic, it is necessary to identify different correlation functions in each direction. This is accounted for by allowing different correlation parameters, θ_i, in two or three dimensions. See Lophaven *et al.*[10,11] for more information about the optimization of the correlation length, the anisotropy issue, and other computational aspects of the procedure.

We have also developed our own Kriging interpolation method based on the variogram model. In general, both correlogram and variogram models give similar results, but currently employing the DACE Toolbox is computationally much more efficient. The reader is referred to Ref. 14 for a discussion about Kriging based on a variogram model.

Recently, Kriging interpolation and POD-based methods have been successfully applied to data recovery and reconstruction of randomly generated laminar gappy flow fields of uniform flow past a circular cylinder (see Refs. 13 and 15). Kriging interpolation has also been applied to large spatial gappiness or for flow fields with black zones with considerable success for relatively smooth data. In this paper, we will apply Kriging interpolation to more complicated, wall-bounded transitional boundary layer flow involving a laminar separation bubble. In addition, a new DNS-based "interpolation" will be introduced to enhance and smooth the experimental data by making use of the POD modes obtained from DNS. Finally, the peculiarities of DNS-based interpolation and Kriging interpolation are discussed.

II. EXPERIMENTAL (PIV) AND NUMERICAL (DNS) DATA

The PIV experiments were carried out by Lang,[16] while the DNS simulations were performed by Marxen.[17] For detailed information on both works, we refer to the aforementioned dissertations. Summaries can be found in Lang *et al.*[18]

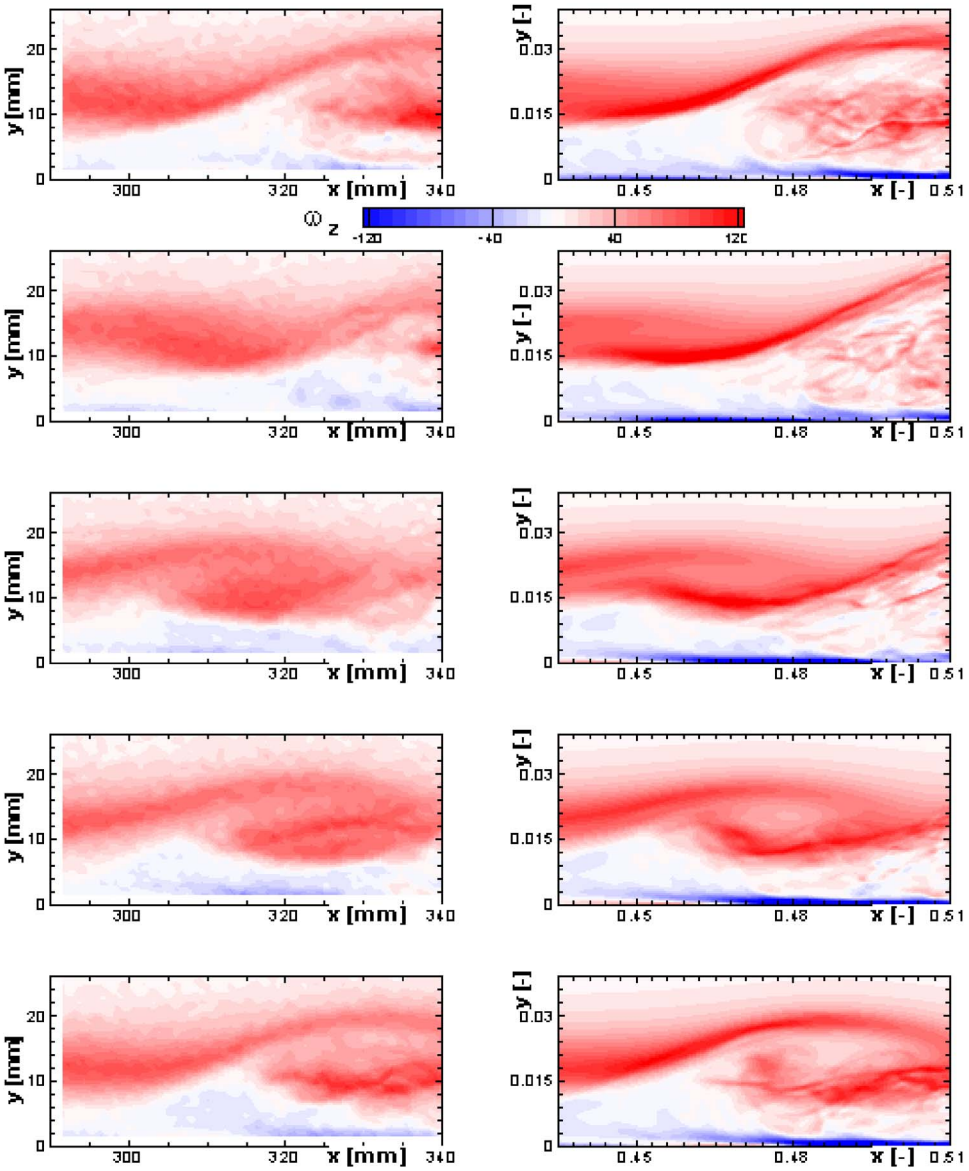

FIG. 1. Contours of the spanwise vorticity at $z=0$ for single time instants (from top to bottom: $t/T_0=0,0.2,0.4,0.6,0.8$). Comparison of phase-averaged results from PIV (Ref. 16) (left) and DNS (Ref. 17) studies (right).

and Marxen and Rist.[19] Here, we briefly inform the reader about the investigated flow problem, nonlinear transition stages of a flat plate boundary layer flow involving a laminar separation bubble. The basic transition scenario is that in which a laminar boundary layer separates in a region of adverse pressure gradient from a flat plate, undergoes laminar-turbulent transition, and reattaches as a turbulent boundary layer to form a laminar separation bubble.

The experiments were performed in a laminar water tunnel facility at the Institute of Aerodynamics and Gas Dynamics in Stuttgart University. A flat plate is mounted in the free stream ($U_\infty=0.125$ m/s) of the test section of a laminar water tunnel. To generate a pressure-induced laminar separation bubble, a displacement body (length of the body $L=0.69$ m) was positioned in the test section above the flat plate. The global Reynolds number based on the displacement body length and the reference velocity ($U_\infty=0.125$ m/s) is $\mathrm{Re}=10^5$ in water. For experimental setup and other detailed information, see Ref. 18. For DNS calculations, general physical parameters of the flow are chosen to match the experimental setup as closely as possible.

The comparison of phase-averaged results both from PIV and DNS are given in Fig. 1 as reported by Marxen and Rist,[19] where instantaneous contours of the spanwise vorticity (ω_z) at the spanwise location $z=0$ are shown in a time periodic signal. As shown in Fig. 1, the instantaneous experimental and numerical results agree closely with each other.

For the purpose of this investigation, a total of 9 snapshots from PIV and a much finer sampling of 50 snapshots from DNS data are used in order to extract the POD modes.

III. EXTRACTION OF POD MODES: PIV-BASED VERSUS DNS-BASED MODES

The POD procedure is now well documented, and therefore we do not repeat it here but state that we implement the snapshot version of POD introduced by Sirovich.[20] We refer to the book by Holmes *et al.*[21] and various papers (Deane *et*

al.,[22] Noack and Eckelman,[23] Rempfer,[24] Liakopoulos *et al.*,[25] Jing *et al.*,[26] Ma and Karniadakis[27]) for a detailed discussion of theoretical and numerical issues of the POD procedure.

Employing the method of snapshots, we have extracted POD modes from datasets corresponding to both the PIV measurements and to DNS. In all of our computations, we extract the POD modes for the *fluctuating* velocity field. We also note that applying POD to the *total* velocity field is also possible. The only difference would be that the most energetic mode (we can call it zero mode) would then contain the mean flow. It is well known that POD modes $\Psi_k(x,y)$ can be used to reconstruct the dataset (from which they are extracted) *optimally* for a given number of N terms as follows:

$$\omega_z(x,y,t) \cong \sum_{k=1}^{N} a_k(t)\Psi_k(x,y), \tag{1}$$

where $a_k(t)$ denotes the temporal coefficients of POD modes. For a given dataset, the maximum number of modes that can be obtained is equal to the number of snapshots, M. However, in general (with the possible exception of turbulent flows), the first few modes capture the most of the energy of the flow, as quantified by the normalized eigenvalues. In other words, in general, the number of POD modes to reconstruct the field variables to an acceptable degree is much lower than the number of snapshots required for a sufficient temporal resolution of the flow.

Equation (1) is called the "reconstruction formula," and since the POD modes are orthogonal by construction, the temporal coefficients $a_k(t)$ can be obtained from Eq. (1) by a "direct projection" formula as

$$a_k(t) = \int_{\Omega} \omega_z(x,y,t),\Psi_k(x,y)d\Omega, \quad k = 1,2,\ldots,N. \tag{2}$$

The above equations relate to the specific example of the spanwise component of vorticity (a scalar field) at a constant spanwise location ($z=0$), but the extension is obvious for a three-dimensional vector field as well. We also report some results on the three-dimensional velocity vector field in the second part of this paper.

Since eigenvalues of the covariance matrix represent the energy content of the modes, we show the distribution of eigenvalues obtained from PIV measurements and DNS in Fig. 2. The comparison of PIV versus DNS eigenvalues shows a remarkable similarity for almost *all* of the modes. In particular, most of the fluctuating kinetic energy is captured by the first four modes for both PIV- and DNS-based modes, i.e., the first four PIV-based modes capture 89.1% while the first four DNS-based modes capture 90.9% of the total energy. Ma *et al.*[5] make a similar comparison of digital PIV and *two-dimensional* DNS results for a flow past a circular cylinder at Reynolds number 610. They report that the fluctuating kinetic energy content of only the first six modes agrees with each other, and for higher modes the energy spectrum of the DNS-based modes decays sharply, while the spectrum of PIV-based modes decreases rather monotonically with a nearly constant slope. They state two probable causes for this discrepancy: (i) the noise and the background

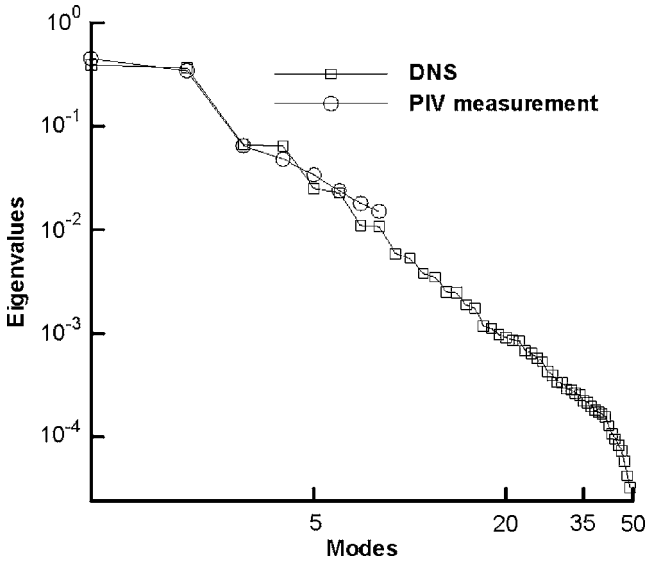

FIG. 2. Comparison of eigenvalues computed from experimental (PIV) and numerical (DNS) results.

turbulence of experimental data, and (ii) limitation of the two-dimensional simulation. They also report that the eigenvalue spectrum for the two-dimensional simulations decays faster compared to three-dimensional simulations. This is in agreement in our 3D simulations, and combining our findings with theirs, we can say that the limitation of the two-dimensional simulation seems to be a major source of the spectrum discrepancy while the noise and the background turbulence of the experimental data seem to play only a minor role.

Figures 3 and 4 show the comparison between PIV- and DNS-based POD modes, while corresponding coefficients of the modes are given in Figs. 5(a) and 5(b), respectively. The comparison of experimental and numerical POD modes (versus time) reveals that the first four most energetic modes show a considerable similarity, while deviations are evident for higher-order modes. It is also noted that for DNS results, well-organized, small-scale coherent structures are observable for even very high-order, low-energy content modes [e.g., the 15th and 19th modes shown in Fig. 4(b)]. The high-order PIV-based POD modes, on the other hand, are noisy. By comparing the coefficients of the PIV- and DNS-based POD modes [Figs. 5(a) and 5(b)], we see that they are quite similar as well but we also note that a mode and a corresponding coefficient "phase shift" in mode pairs is observable, as already reported in Prabhu *et al.*[3] and Gunes and Rist[2], for instance.

IV. RECONSTRUCTION OF PIV DATA

A. Reconstruction of PIV data via PIV-based POD modes

In order to compare and assess the differences, we will use both PIV- and DNS-based modes in reconstructing the original PIV data. Next, we will investigate noise filtering (smoothing) and the possibility of enhancement of the spatial resolution of original PIV data.

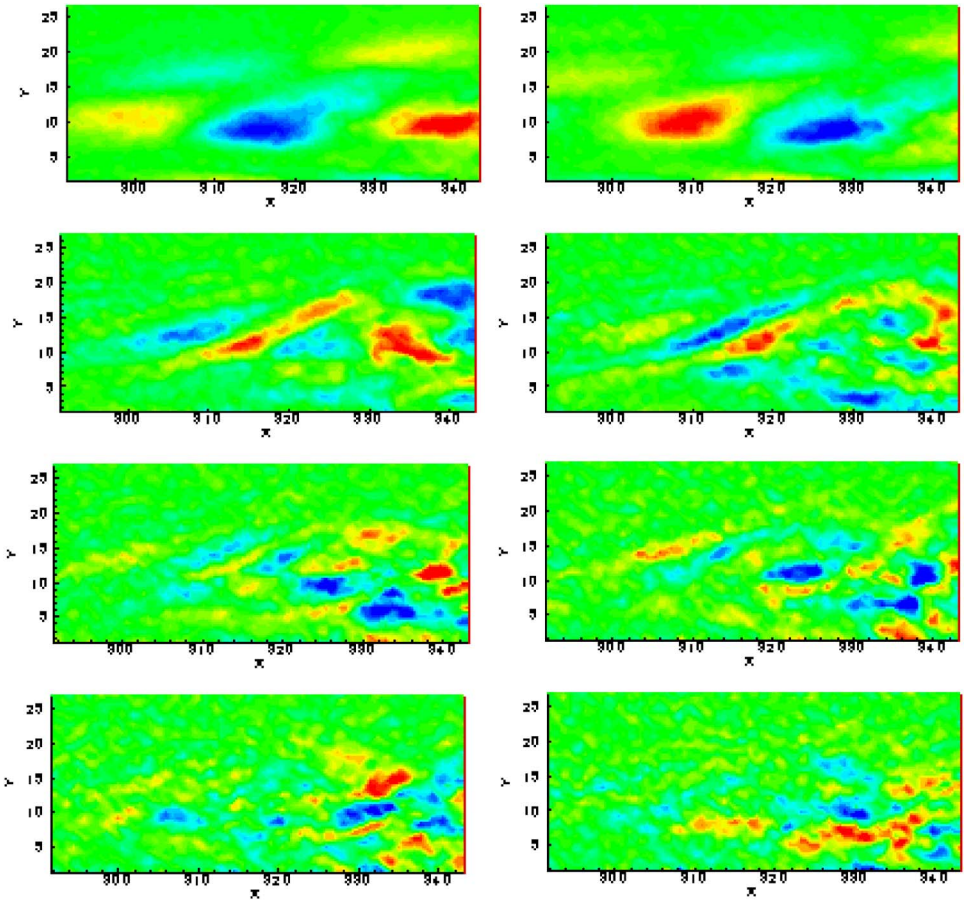

FIG. 3. The eight most energetic PIV-based POD modes of spanwise vorticity (left column: odd number modes, right column: even number modes).

Let us write the decomposition of the PIV dataset utilizing both PIV- and DNS-based modes:

$$\omega_z^{\mathrm{PIV}}(x,y,t) \cong \sum_{k=1}^{N} a_k^{\mathrm{PIV}}(t)\Psi_k^{\mathrm{PIV}}(x,y), \tag{3}$$

$$\omega_z^{\mathrm{PIV}}(x,y,t) \cong \sum_{k=1}^{N} a_k^{\mathrm{model}}(t)\Psi_k^{\mathrm{DNS}}(x,y), \tag{4}$$

where the model coefficients a_k^{model} can be calculated by a cross projection of the DNS-based modes on the PIV data as

$$a_k^{\mathrm{model}}(t) = \int_{\Omega} \omega_z^{\mathrm{PIV}}(x,y,t),\Psi_k^{\mathrm{DNS}}(x,y)d\Omega. \tag{5}$$

Figure 6(a) shows the reconstruction of a representative instantaneous snapshot of the experimental spanwise vorticity (PIV data) for a different number of PIV-based POD modes (direct projection). The original PIV data are shown for comparison. It is seen that only the first five modes are sufficient for an accurate reconstruction (with an rms error of 0.1204) since PIV-based modes are optimal for the experimental data. It is also noted that because PIV-based modes contain experimental noise (see Fig. 3), the reconstructed PIV data (spanwise vorticity field) are as noisy as with the original PIV data. Here, in order to smooth the PIV data, we first employ the Kriging procedure on the noisy POD modes, and reconstruct the original data with optimal but *smoothed* PIV-based modes as shown in Fig. 6(b). As all the PIV-based modes are smoothed (including the average PIV data-mode zero), the reconstruction results in smooth data fields for any selected number of modes. It is seen in Fig. 6(b) that the first five smoothed POD modes accurately capture the PIV data (with an rms error of 0.1960). The reconstruction error as a function of mode numbers is given in Table I. We note that, while using all the original modes leads to zero reconstruction error, hence containing the noise as well, the smoothed modes result in a converged rms error of 0.1701. So, this difference is obviously due to the removal of the noisy part of the data. We show in Fig. 7(a) the smoothed POD modes (they may be compared with the original POD modes in Fig. 3).

Since the POD modes are smoothed, they are expected to no longer be orthogonal (relative to the scalar product that was used when the original/noisy POD modes were determined) and optimal. Therefore, as suggested by one referee, we also considered smoothing the PIV data first, and then determining POD modes for the smoothed PIV data. The resulting eight most energetic *orthogonal* set of POD modes obtained for the *smoothed* PIV data is shown in Fig. 7(b). The orthogonal set of POD modes is crucial if one is required to construct an accurate low-dimensional model to investigate the characteristics of the dynamical system. However, for the data reconstruction/smoothing and interpolation purposes, as implemented in the current paper, the POD modes may not be required necessarily to be orthogonal. In addition, we think that smoothing POD modes, rather than smoothing PIV data itself (i.e., this requires all snapshots to

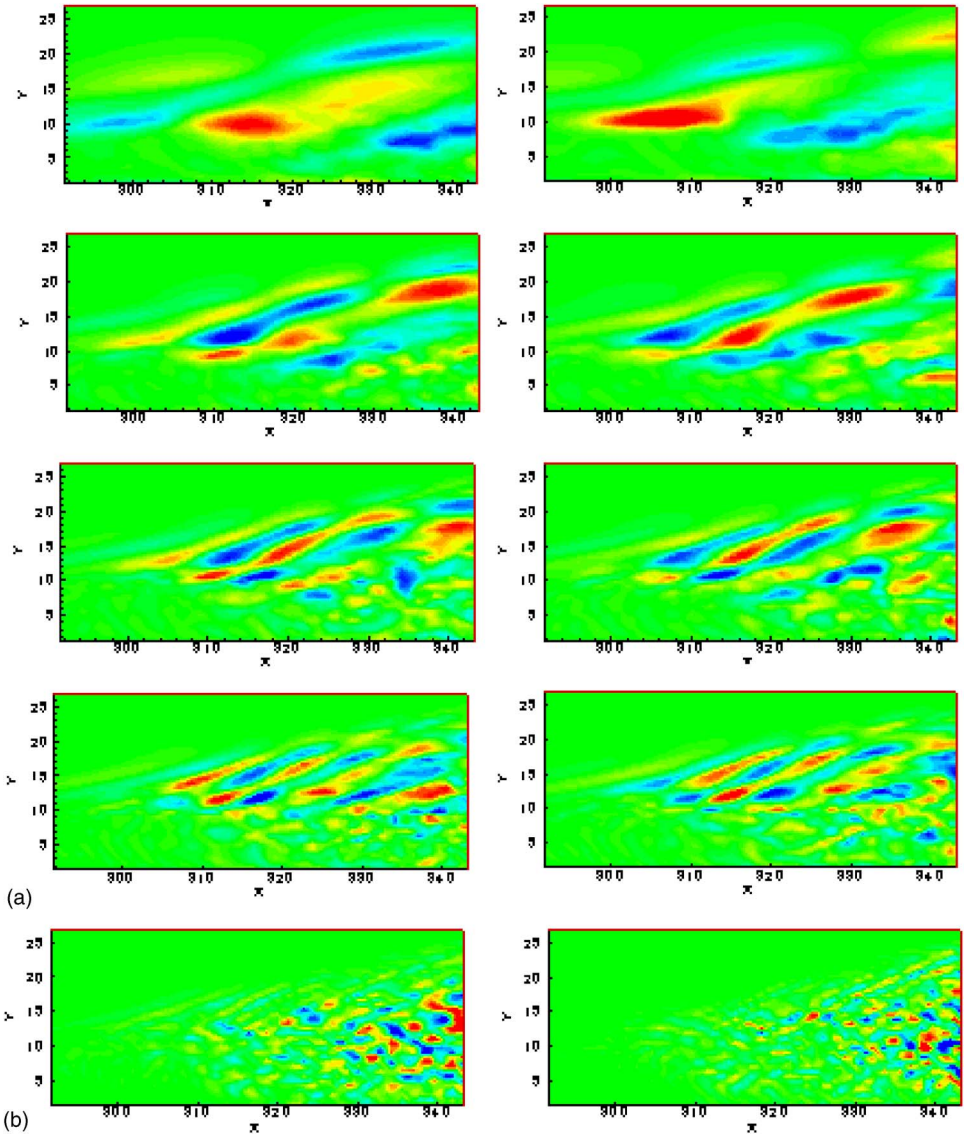

FIG. 4. (a) The eight most energetic DNS-based POD modes of spanwise vorticity (left column: odd number modes, right column: even number modes). (b) Higher order DNS-based POD modes. The 15th (left) and 19th (right).

be smoothed separately), might have the following advantages:

(i) POD leads to a natural separation of the large scales from the small ones (low-order modes contain large scales and high-order modes small scales) and at the same time there is a good separation of the coherent part (low-order modes) from the incoherent part (higher-order modes).

(ii) Smoothing of each snapshot before performing the POD requires more computer time and contains the danger that large and coherent structures are more affected by the smoothing procedure than in our case.

(iii) Smoothing of the large-scale structures will not deteriorate the small-scale structures, and vice versa.

(iv) When the smoothing is performed individually for each snapshot, due to instantaneous flow complexity and/or measurement errors, the noise content of some snapshots may be quite different from the rest and, therefore, it is difficult to control and adjust the smoothing parameter for each snapshot, i.e., it is likely that some snapshots are too much (oversmoothed) or too little smoothed, which in turn will affect the POD modes.

For the problem at hand, comparing orthogonal and nonorthogonal POD modes, the most energetic four modes are very close to each other, while there is a considerable difference in less energetic higher-order modes [see Figs. 7(a) and 7(b)]. Also, Table II shows the energy content of each orthogonal/nonorthogonal POD mode. While the first four orthogonal/optimal modes capture 94.71% of the flow fluctuating energy, the nonorthogonal/nonoptimal modes capture 90.95% of the same energy. We can conclude that while the orthogonality property of the POD modes is eliminated theoretically by smoothing the modes, especially the most energetic POD modes are not "far away" from the orthogonality condition when they are smoothed.

In addition, in smoothing PIV data first, there is a danger that small-scale important features of the flow (higher-order structures) may be confused with noise and lost along with the latter during the smoothing process. Actually, we investigate Kriging interpolation/smoothing in Sec. V in detail and show that by controlling the correlation parameter, one can choose the degree of smoothness for the Gaussian correlation function (see, for example, Fig. 17).

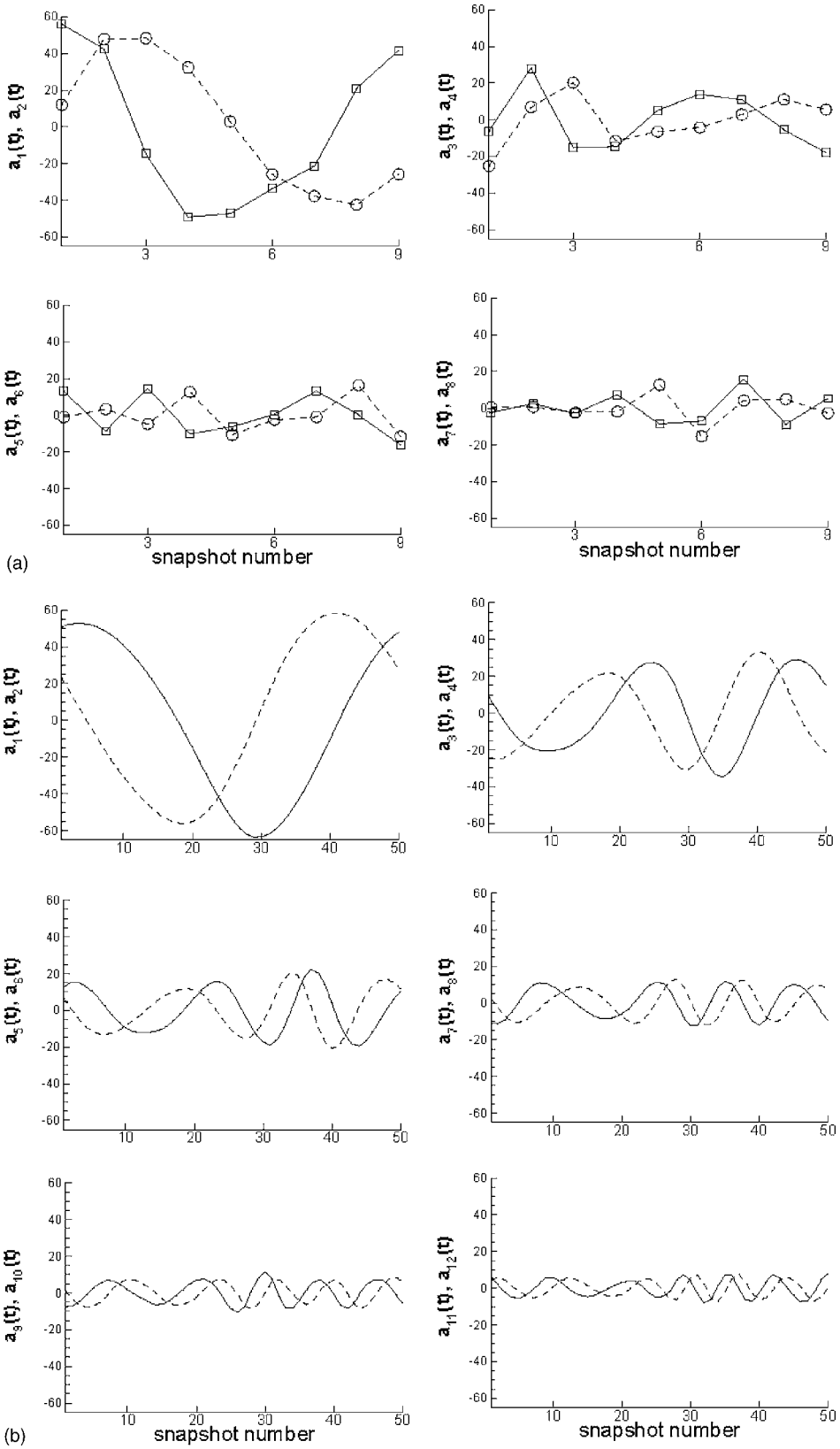

FIG. 5. Coefficients of (a) PIV-based POD modes, (b) DNS-based POD modes

Finally, in Table I, we compare the reconstruction errors as a function of PIV-based mode number. The reconstruction error for both procedures, i.e., mode-smoothing and PIV-data smoothing, give similar results for low-order modes (for the two most energetic pairs), while there is some difference if one considers other (high-order) modes. This is in agreement with the fact that the four most energetic *smoothed* POD modes and POD modes obtained from *smoothed* PIV data resemble each other, as shown in Figs. 7(a) and 7(b).

As a concluding remark in this section, there is no clear advantage for one or the other procedure (perhaps apart from the argument of computer time, especially when a larger

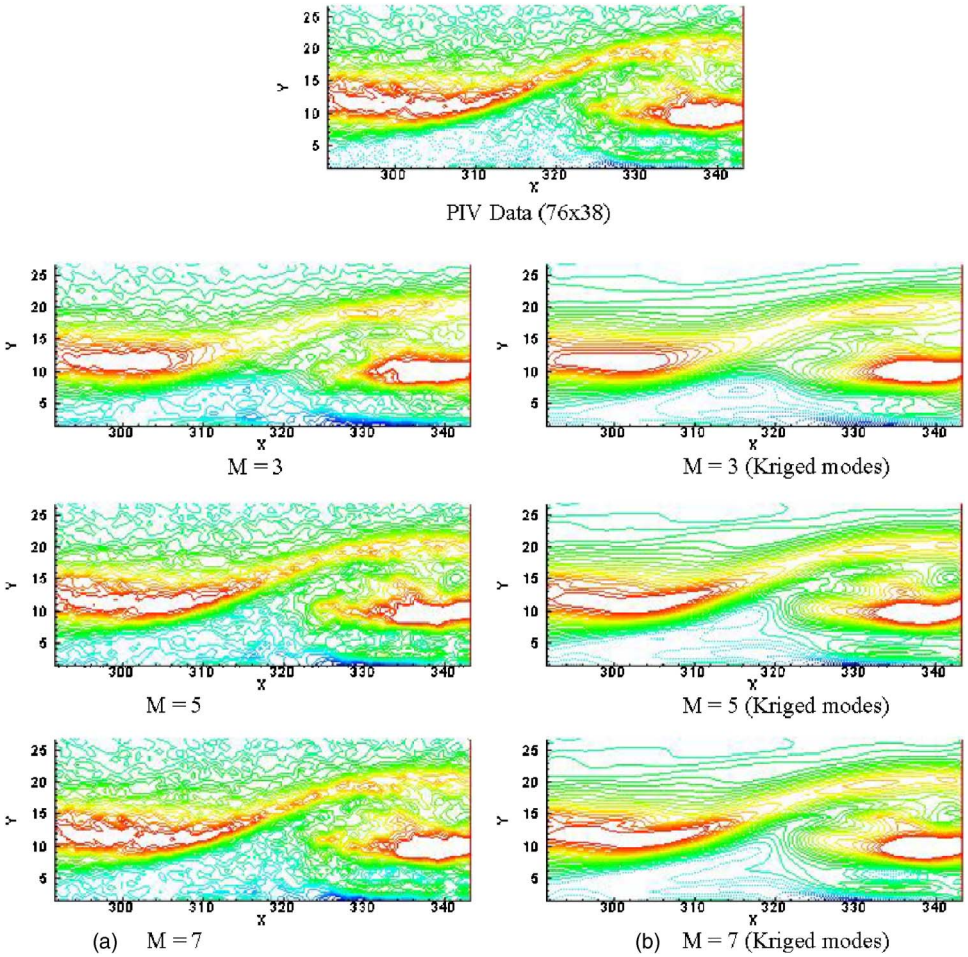

FIG. 6. Reconstruction of PIV data using PIV-based POD modes (direct projection). (a) Original (noisy) PIV-based POD modes, (b) PIV-based POD modes *smoothed* by the Kriging procedure.

number of snapshots are available). Both methods can be used depending on the application. For data reconstruction/smoothing and interpolation, mode-smoothing may be appropriate while PIV-data smoothing shall be employed for low-dimensional representation of flow data, which requires orthogonal POD modes.

TABLE I. Reconstruction error as a function of PIV-based mode number. Smoothed POD modes are obtained by the Kriging procedure (middle column), while in the right column, we smooth PIV data first, and then determine POD modes for the smoothed PIV data.

	Reconstruction error		
Mode number	Using original POD modes	Using smoothed POD modes	Using smoothed PIV data
2	0.2798	0.2927	0.2956
3	0.2597	0.2737	0.2751
4	0.2536	0.2714	0.2740
5	0.1204	0.1960	0,2274
6	0.0247	0.1715	0.1928
7	0.0226	0.1713	0.1888
8	0.0040	0.1701	0.1876
9	0.0	0.1701	0.1876

B. Reconstruction of PIV data via DNS-based POD modes

In the preceding section, we have shown that PIV data can be reconstructed and smoothed effectively employing PIV-based POD modes along with the Kriging procedure. In this section, we will investigate the possibility of reconstruction of PIV data employing DNS-based POD modes. This task is important because in many instances, the experimental data have very low resolution or are only partially available, and extracting additional information/data from available DNS data can be highly desirable. Before employing DNS-based modes to reconstruct PIV data, for a comparison we present reconstruction of the DNS data using DNS-based modes in Fig. 8 (direct projection). Similar to the PIV data, the DNS data are reconstructed with few modes accurately (with an rms error of 0.2333 for the first five modes). We also note the noise-free spatial distribution of the reconstruction as expected.

Having mentioned that PIV- and DNS-based modes are only optimal for their corresponding data, we will now investigate reconstruction, smoothing, and spatial resolution enhancement of PIV data employing (theoretically nonoptimal but closely related) DNS-based modes. As reported by Prabhu *et al.*,[3] the "cross projection" represents the ability of

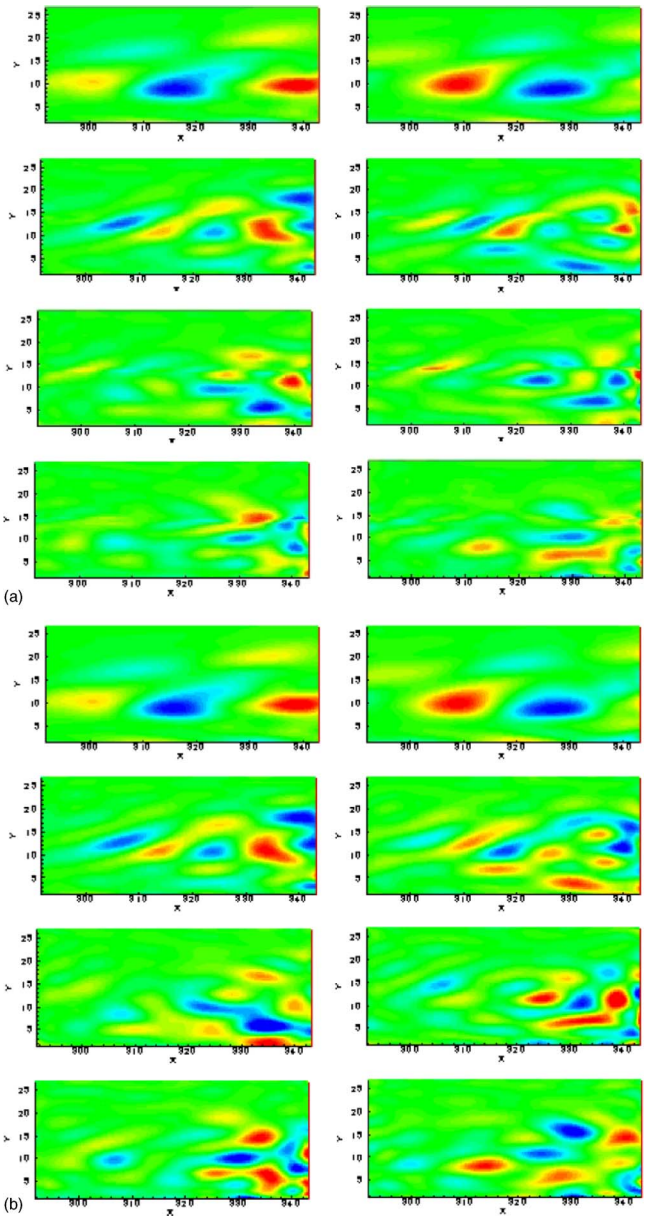

FIG. 7. (a) The eight most energetic PIV-based *smoothed* (nonorthogonal) POD modes of spanwise vorticity (left column: odd number modes, right column: even number modes). (b) Orthogonal set of POD modes obtained for the smoothed PIV data (left column: odd number modes, right column: even number modes).

nonoptimal POD modes (here DNS-based modes) to describe the actual PIV data. Therefore, by reconstructing the spanwise vorticity ω_z^{PIV} using Eq. (4), we can evaluate *a priori* the potential of DNS-based modes in reconstructing the PIV data. If DNS-based modes can be used for reconstruction, it is predicted that only the few most energetic modes are necessary for the reconstruction since it has been shown previously that almost 90% of the energy is captured by the first four modes both for PIV and DNS data.

The cross projection formula to evaluate the model coefficients [Eq. (5)] actually requires all PIV data (i.e., ω_z^{PIV} for all points) to be supplied in order to calculate the model coefficients, and the equation implicitly assumes that the DNS-based modes satisfy the orthogonality condition on the

TABLE II. The energy content (in percent) of orthogonal and nonorthogonal POD modes.

Mode number	Orthogonal POD modes	Nonorthogonal POD modes
1	48,41	45,08
2	36,56	34,58
3	5,85	6,49
4	3,89	4,80
5	2,09	3,40
6	1,38	2,38
7	1,02	1,80
8	0,80	1,51

PIV measurement points (domain). On the other hand, in order to calculate the model coefficients, a least-squares method proposed by Gunes and Rist[2] may be used for a partially available or very coarse PIV dataset (e.g., data with missing zones) and the method does not require that DNS-based modes are orthogonal. That is, by providing flow data only at selected locations $(x_i y_i)$ and employing a least-squares fit on Eq. (4), one can calculate the model coefficients without requiring the use of Eq. (5). Particularly, we can write a least-squares error as

$$E = \min\left[\sum_{k=1}^{P}\left\{\left(\sum_{j=1}^{N} a_j \Psi_{j,k}^{\mathrm{DNS}}\right) - \omega_{z,k}^{\mathrm{PIV}}\right\}^2\right] \tag{6}$$

and a least-squares fit formulation reduces to the following system of algebraic equations for the model coefficients:

$$\begin{bmatrix} \sum_{k=1}^{P}\Psi_{1,k}^2 & \sum_{k=1}^{P}\Psi_{2,k}\Psi_{1,k} & \cdots & \sum_{k=1}^{P}\Psi_{N,k}\Psi_{1,k} \\ \sum_{k=1}^{P}\Psi_{1,k}\Psi_{2,k} & \sum_{k=1}^{P}\Psi_{2,k}^2 & \cdots & \sum_{k=1}^{P}\Psi_{N,k}\Psi_{2,k} \\ \cdots & & & \\ \sum_{k=1}^{P}\Psi_{1,k}\Psi_{N,k} & \sum_{k=1}^{P}\Psi_{2,k}\Psi_{N,k} & \cdots & \sum_{k=1}^{P}\Psi_{N,k}^2 \end{bmatrix} \begin{bmatrix} a_1^{\mathrm{model}}(t) \\ a_2^{\mathrm{model}}(t) \\ \cdots \\ a_N^{\mathrm{model}}(t) \end{bmatrix} = \begin{bmatrix} \sum_{k=1}^{P}\omega_{z,k}^{\mathrm{PIV}}(t)\Psi_{1,k} \\ \sum_{k=1}^{P}\omega_{z,k}^{\mathrm{PIV}}(t)\Psi_{2,k} \\ \cdots \\ \sum_{k=1}^{P}\omega_{z,k}^{\mathrm{PIV}}(t)\Psi_{N,k} \end{bmatrix}. \tag{7}$$

In Eq. (7), P denotes the total number of data points in the PIV measurements while N denotes the number of most energetic *DNS-based* POD modes and determines the size of the coefficient matrix. The PIV data are utilized to evaluate the right-hand side (RHS) of the linear system, while the coefficient matrix is computed once and for all from DNS data. The size of the linear system depends on the number of

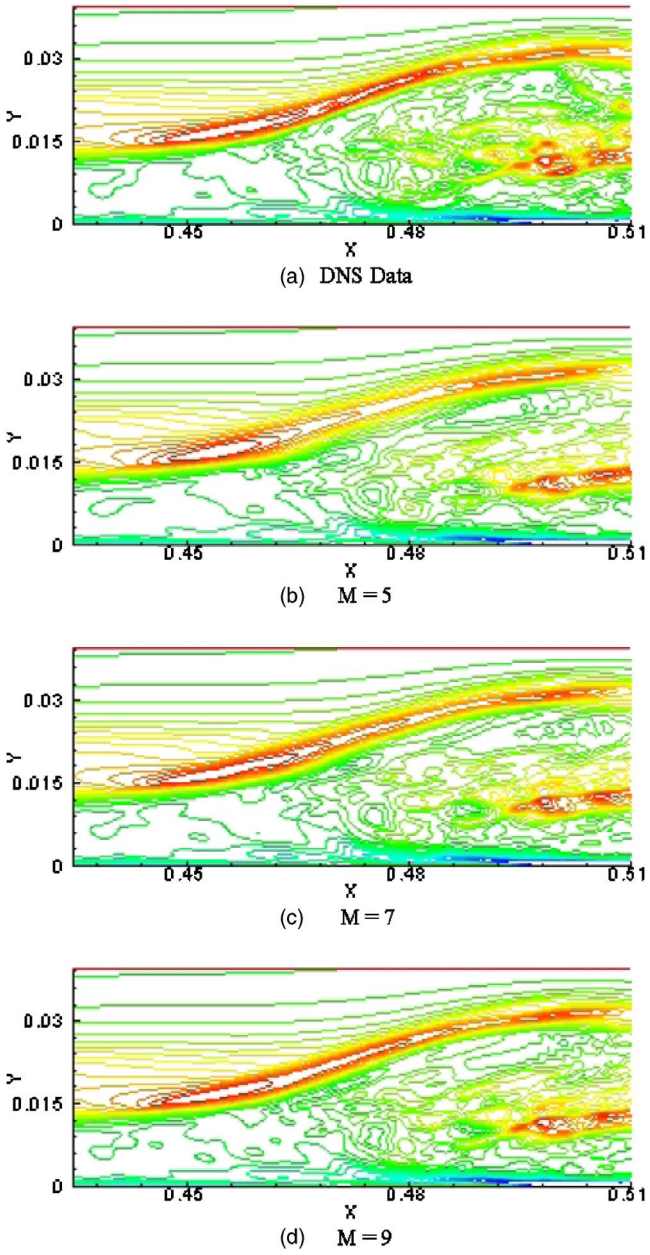

FIG. 8. Reconstruction of DNS data via DNS-based modes (direct projection). (a) Original DNS data, (b) five DNS-based modes, (c) seven DNS-based modes, (d) nine DNS-based modes.

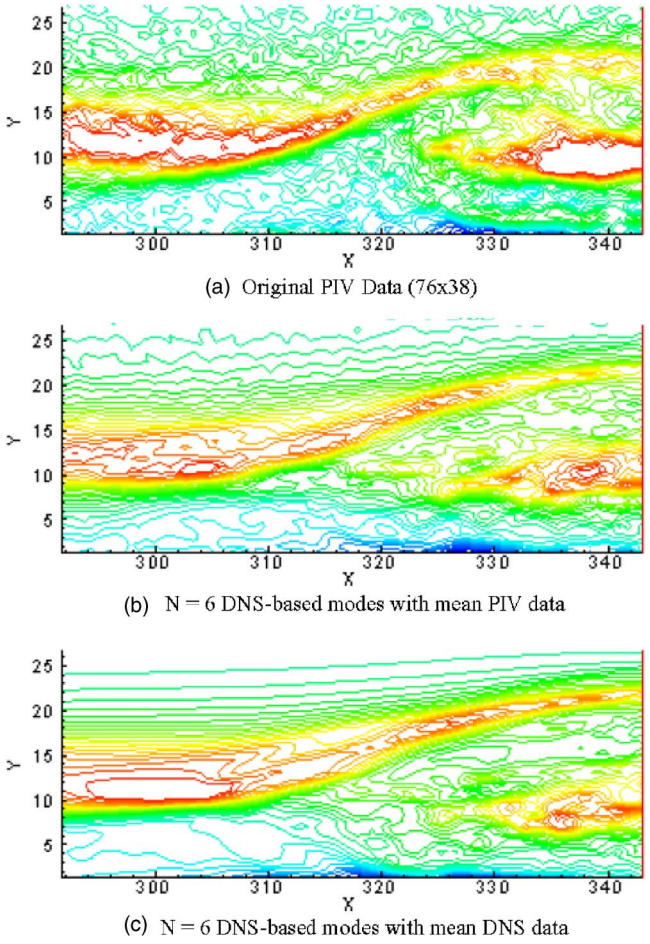

FIG. 9. The effect of the mean flow in reconstructing PIV data via DNS-based POD modes (cross-projection with the least-squares approach).

modes used in Eq. (4). By employing a triangular decomposition, the hybrid model coefficients can be calculated efficiently for different PIV data sets.

In order to investigate the performance of each reconstruction procedure in detail, we employ the root mean square (rms) error for *each snapshot* as follows:

$$\mathrm{rms}^N(\omega_z) = \frac{\sqrt{\frac{1}{TN}\sum_{i=1}^{TN}[\omega_{z,C}^N(x,y) - \omega_z(x,y)]^2}}{\sqrt{\frac{1}{TN}\sum_{i=1}^{TN}[\omega_z(x,y) - \varpi_z]^2}}, \tag{8}$$

where TN is the total number of nodal points in the flow field, $\omega_{z,C}^N$ denotes the reconstructed spanwise vorticity via N

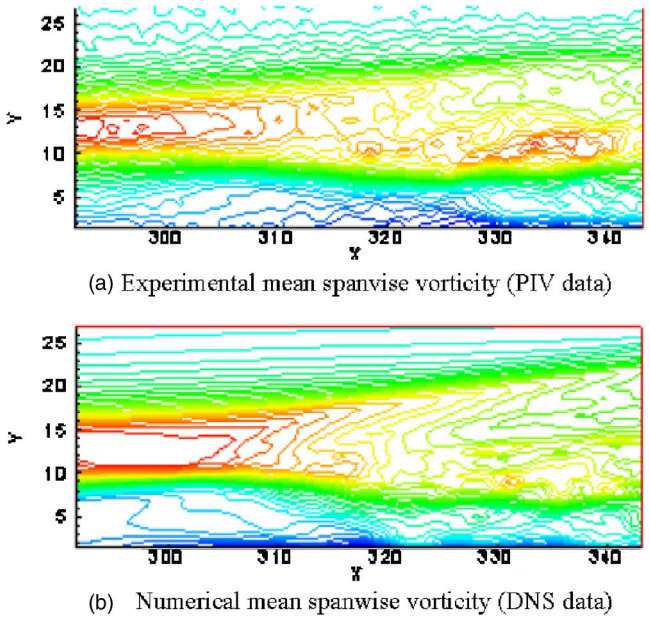

FIG. 10. Comparison of mean spanwise vorticity of PIV and DNS data.

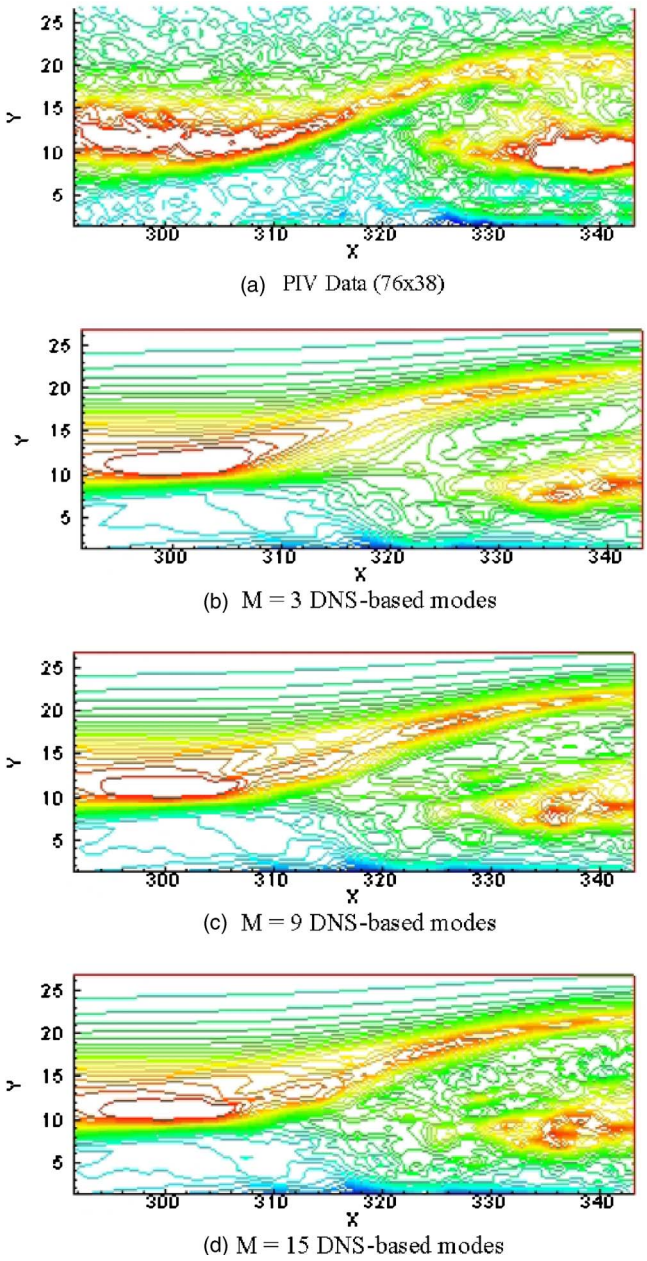

FIG. 11. Reconstruction of PIV data with various numbers of DNS-based POD modes (via the least-squares approach).

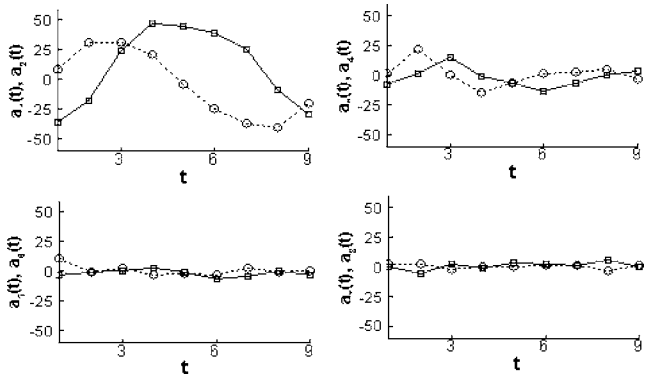

FIG. 12. The model coefficient as obtained by the least-squares approach.

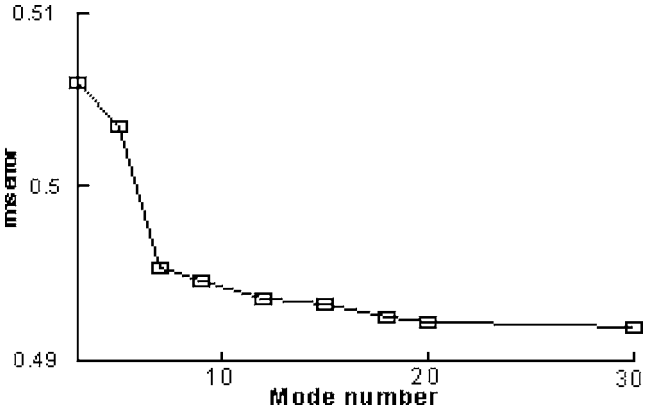

FIG. 13. The rms error of reconstruction for PIV data as a function of DNS-based POD modes (with the least-squares approach).

modes, while $\omega_z(x,y)$ denotes the "actual" spanwise vorticity obtained from the PIV measurements. Note that in order to normalize with respect to the "variance" of the field, we evaluate the variance as

$$\sqrt{\frac{1}{TN}\sum_{i=1}^{TN}[\omega_z(x,y)-\varpi_z]^2}, \tag{9}$$

where ϖ_z is the *average* of the PIV vorticity field, $\omega_z(x,y)$. We also note here that using a relative error is not particularly suitable here because at some (but only few) points, the field values are so small that small deviations give very large relative errors, which make a reasonable comparison impossible.

Figure 9 shows the reconstruction of the PIV data employing (N=6) DNS-based POD modes obtained by the least-squares approach. For a comparison, we also show the original PIV data at the top of the figure. It is important to note that the extracted POD modes (shown in Figs. 3 and 4) are for the fluctuating part of the vorticity. To visualize the instantaneous vorticity, the *mean* vorticity needs to be added. The mean vorticity contours shown in Fig. 10 for both PIV and DNS datasets are very similar. However, we still notice some background noise for PIV data as expected. (It is possible to smooth the mean vorticity employing Kriging). Therefore, we prefer the mean vorticity from DNS for two reasons: (i) it eliminates the background noise associated with the PIV measurements, (ii) in a case in which only partial measurements are at hand in a domain of interest, the mean experimental velocity cannot be used. Therefore, in all

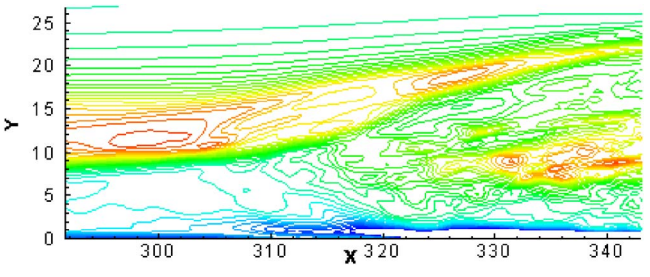

FIG. 14. Spatial resolution enhancement of PIV data to a fine DNS grid of (116×156) using nine DNS-based POD modes.

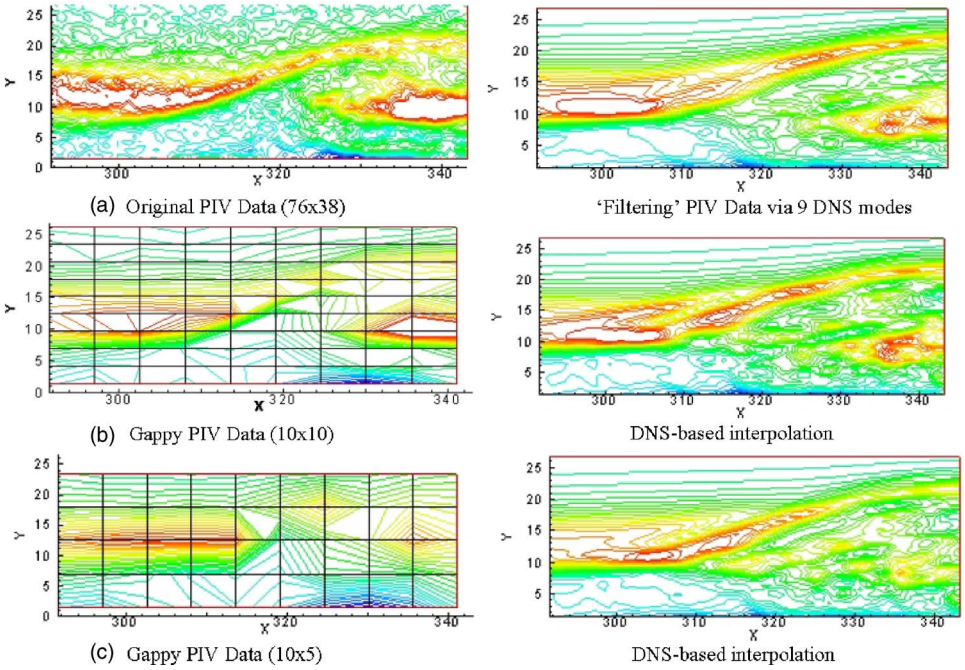

FIG. 15. Resolution enhancement of "gappy" PIV data using nine DNS-based POD modes. The left column shows the gappy PIV data (obtained by discarding a significant part of the available PIV data), and the right column shows the enhancement of PIV data via DNS-based POD modes. The "DNS-based" interpolation refers to using POD modes extracted from DNS in the reconstruction of gappy PIV data.

the reconstructions in this paper that follow, we use the *DNS* mean spanwise vorticity.

The effect of the number of DNS-based POD modes on the reconstruction of PIV data is shown in Fig. 11. We see that the shear layer due to laminar separation is captured by only the first few modes. The model coefficients obtained from the least-squares approach [Eq. (7)] are given in Fig. 12. These coefficients are used along with the DNS-based

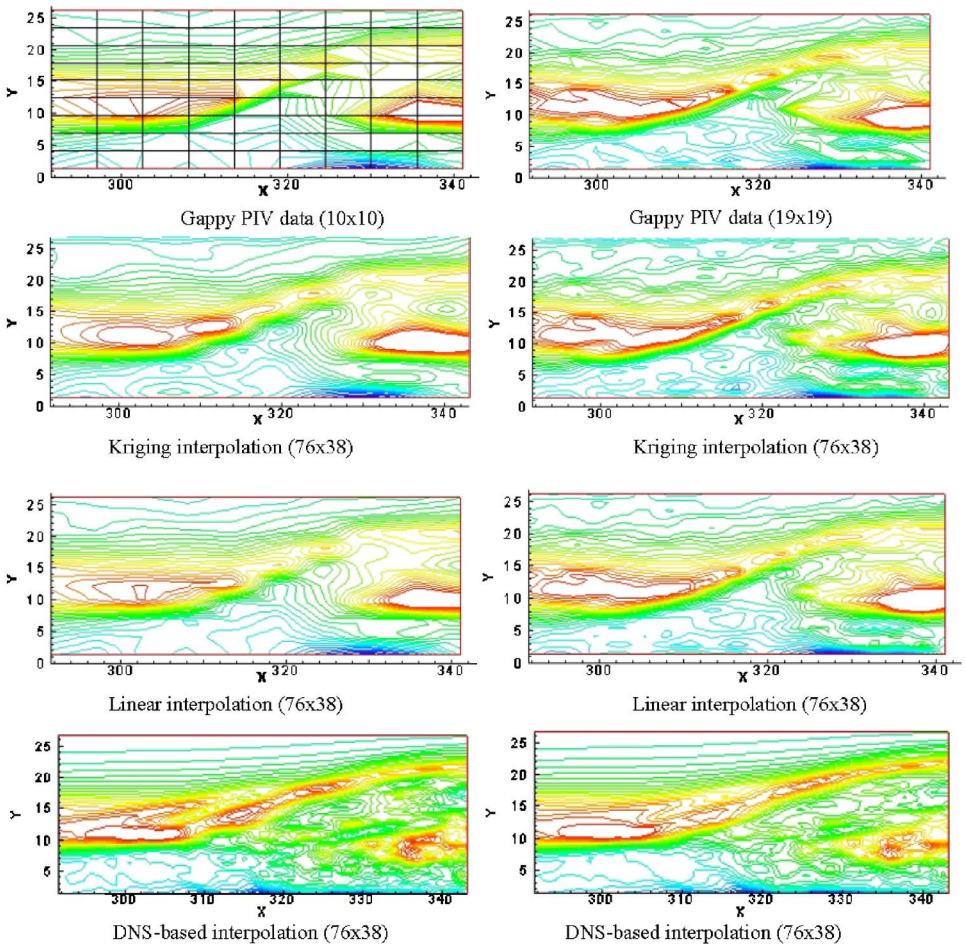

FIG. 16. The enhancement of the gappy PIV data using various procedures.

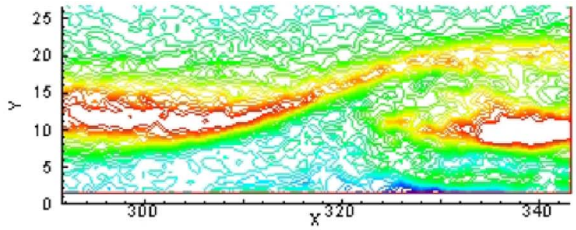

(a) Original PIV data (to Krig) (76x38)

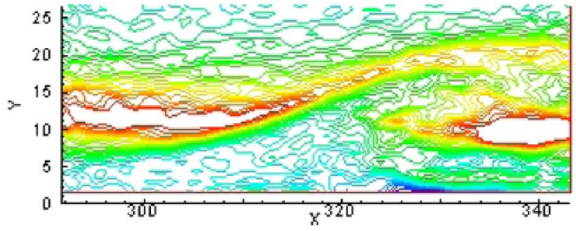

(b) Kriging with correlation parameter, [θ_x=7, θ_y=7] (76x38)

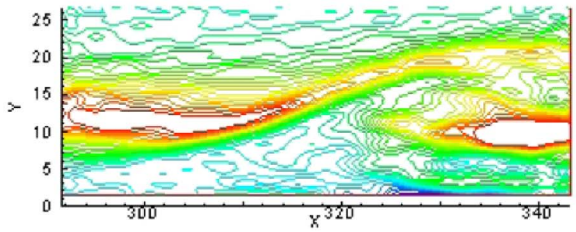

(c) Kriging with correlation parameter, [θ_x=3, θ_y=3] (76x38)

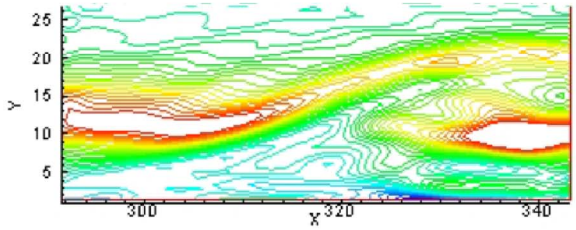

(d) Kriging with correlation parameter, [θ_x=1, θ_y=1] (76x38)

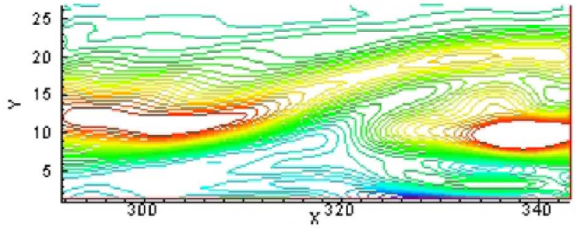

(e) Kriging with (optimized) correlation parameter, [θ_x=0.31, θ_y=0.62] (76x38)

FIG. 17. Kriging interpolation of experimental data for various values of correlation parameters.

POD modes in order to reconstruct PIV data shown in Fig. 11. The reconstruction rms error, defined in Eq. (8) as a function of mode number, is given in Fig. 13. The error decreases sharply with the first few modes and levels off to a constant value for higher modes. That is, higher-order DNS-based modes have almost no contribution in reconstructing PIV data, while they *all* contribute in reconstructing DNS data.

Here, an explanation of the computational requirement is appropriate. In order to be able to compute the model coefficients either from Eq. (5) or Eq. (7), the DNS-based POD modes should be obtained on the *experimental* (*PIV*) grid. To achieve this, we first interpolate high spatial resolution DNS data (spanwise vorticity) onto the low spatial resolution PIV data. Then, applying the POD procedure, DNS-based modes are obtained on the PIV measurement points. Note that once the model coefficients are obtained using either Eq. (5) or Eq. (7), they are independent of the spatial variations, thus they can be used with *high spatial resolution* DNS-based modes in order to obtain high-resolution PIV data. Therefore, we compute again DNS modes, now on a finer computational grid. Figure 14 shows the spatial resolution enhancement/smoothing of PIV data to a fine DNS grid of (116×156) using nine DNS-based POD modes. This procedure can be thought as a novel "DNS-based" interpolation employing DNS-based POD modes. In addition, notice that the wall and the near-wall vorticity, not available in the original PIV measurements, are also accurately predicted by this procedure since DNS-based modes contain this information. In this particular measurement campaign of Lang[16], the spanwise vorticity at the $z=0$ plane had been obtained on a fine "experimental grid" (76×38). However, full three-dimensional measurement campaigns carried out with stereoscopic PIV were much coarser (e.g., only nine planes in wall-normal direction). Therefore, in order to see whether DNS-based interpolation works for coarser measurements points, so-called "*gappy*" PIV data were generated artificially by omitting data points from present PIV snapshots. Figure 15 shows the resolution enhancement/smoothing of the gappy PIV data using nine DNS-based POD modes. We refer to the procedure as "DNS-based" interpolation, which means we use smooth (noise-free) POD modes extracted from DNS in the reconstruction of gappy PIV data. It is seen that DNS-based POD modes can be used to extract the important features of the experimental data, not available in the low-resolution gappy PIV data. In fact, the performance of DNS-based interpolation is particularly pronounced for PIV data with a very high gappiness (10×5), as shown in Fig. 15.

V. KRIGING INTERPOLATION

A. Kriging interpolation of PIV data

In our study, we employ a *Gaussian correlation model* since the flow field is continuously differentiable and we would like to smooth the experimental data. We also used other correlation models (e.g., exponential, linear, spherical) and found out that the Gaussian correlation model is necessary for smoothing. The regression model used in all of our studies is based on second-order polynomials. Each time-snapshot is treated as separate data and therefore a separate regression and correlation model may be used for each snapshot, if required. Although Kriging based on a surrogate model is almost always used for interpolation, it can also be used for extrapolation, i.e., the surrogate model can estimate a value at points both inside and outside the neighborhood of the design dataset. Obviously, the interpolated values are much more accurate than the extrapolated values. In fact, our

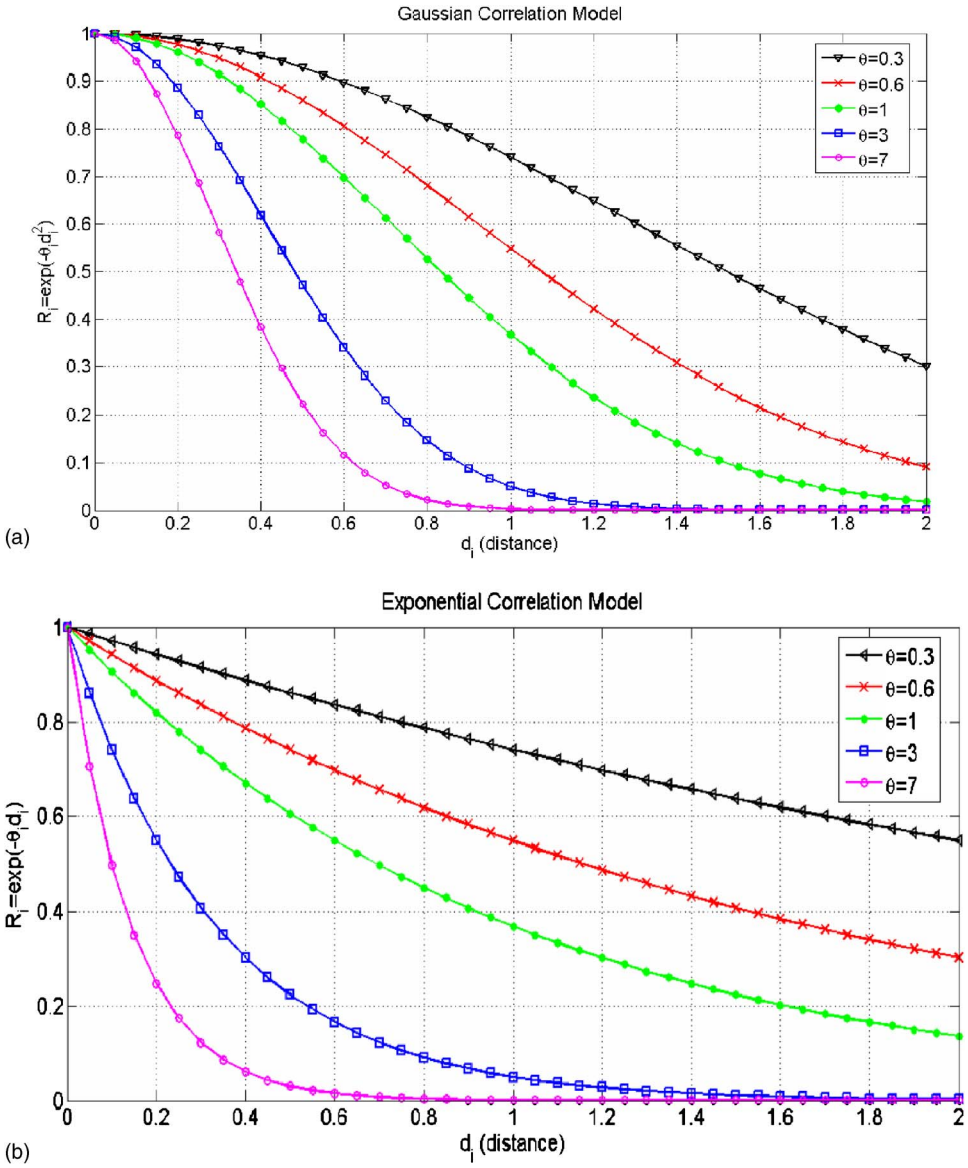

FIG. 18. Variation of the correlation functions with the correlation parameter: (a) Gaussian function, (b) exponential function.

numerical experiments show that the accuracy sharply deteriorates outside the design dataset.

In order to compare to the DNS-based "interpolation," we carried out Kriging interpolation as well as linear interpolation of low-resolution gappy PIV data. Figure 16 shows the reconstruction of the two gappy PIV data sets, (10×10) and (19×19), respectively. For very coarse (10×10) gappy PIV data, DNS-based interpolation is certainly superior to Kriging and linear interpolation. This is an expected result with very low-resolution gappy PIV data, since both Kriging and linear interpolations use only available gappy PIV measurements, and there is simply not enough information to extract the hidden features of the flow. On the other hand, the prediction of Kriging interpolation is improved significantly for the second gappy PIV data with (19×19) resolution, while the prediction of DNS-based interpolation does not change practically. Kriging interpolation of noisy PIV data for various values of the correlation parameters θ_i is shown in Fig. 17. As can be seen, the correlation parameter given in the Gaussian correlation function $R_i=\exp(-\theta_i d_i^2)$ is related to the correlation length and it is crucial for the Kriging interpolation of noisy data. Actually, by controlling the correlation parameter, one can choose the degree of smoothness for the Gaussian correlation function (see Fig. 17). Figure 18(a) shows the variation of Gaussian correlation function with the correlation parameter. The correlation increases as the correlation parameter decreases, i.e., the points in a larger region contribute to the evaluation of the unknown points resulting in a smoother "average" data. We also note that Fig. 17(f) shows the Kriging interpolation with the optimized coefficients. Here, the anisotropy is accounted for in the different values of correlation parameter for each direction. The correlation parameter in the streamwise direction is $\theta_x=0.31$, while in the wall normal direction it is $\theta_y=0.62$ [see Fig. 18(a)]. So, the PIV data in the streamwise direction are more correlated, as expected. Thus, the experimental noise in PIV data is eliminated and a very smooth data field is obtained with Kriging interpolation based on the Gaussian correlation function. On the other hand, we also performed Kriging interpolation based on the

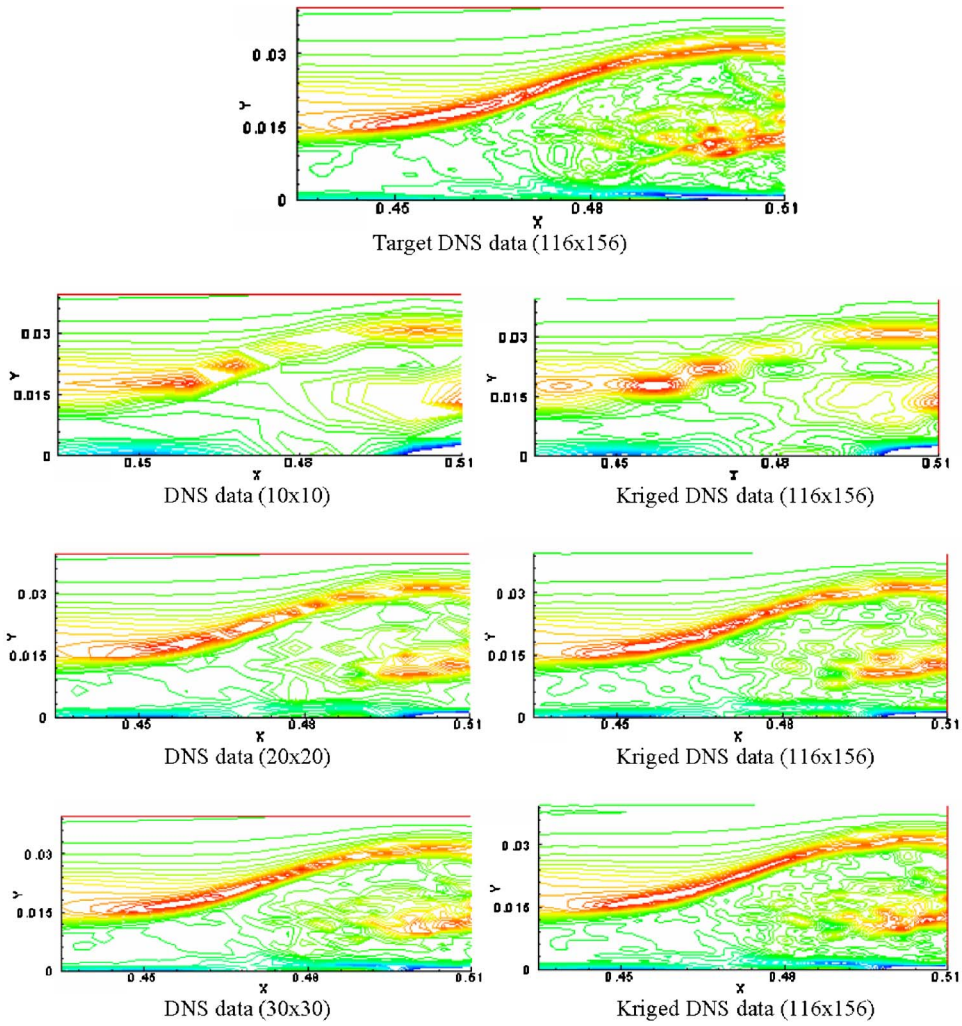

FIG. 19. Reconstruction of gappy data via Kriging interpolation. At the top, target DNS data are shown for visual comparison.

exponential correlation function, $R_i=\exp(-\theta_i d_i)$. Surprisingly, no smoothing at all could be achieved when we used the exponential correlation function for all the correlation parameters, i.e., all the correlation parameters investigated for the exponential function resulted in the "original" noisy PIV data. This includes the computed "anisotropic" optimized correlation parameters $[\theta_x=2.8,\ \theta_y=4.8]$ as well as a range of correlation parameter inputs between $\theta=0.01$ and 10. This may be explained by the parabolic behavior of the Gaussian function near the origin compared to the linear behavior of exponential function as shown in Fig. 18(b).

B. Kriging interpolation of DNS data

In order to compare and quantify the reconstruction error, we have also applied the Kriging interpolation to DNS data. Similar to PIV data, we omitted the values of the vorticity on most nodes and obtained *three* "gappy" DNS datasets consisting of equidistant (10×10), (20×20), and (30×30) grids. Figure 19 shows the contours of the gappy DNS data (left column) and the corresponding reconstructed contours of the vorticity by Kriging interpolation (right column). At the top of the figure, "targeted" original DNS data are shown for visual comparison. To quantify the accuracy of the reconstruction, the rms errors, defined similarly as in Eq. (8) over the computational domain, are given in Table III. Obviously, the local error varies at each point, as shown in Fig. 20. It is noted that for the flow with high gappiness ratio (10×10), the reconstruction error is concentrated in the shear layer, close to the wall and in the downstream part of the separation bubble. On the other hand, for the flow with medium and low gappiness ratios, i.e., gappy data with (20×20) and (30×30), the shear layer is reconstructed virtually free of error, while only a small reconstruction error is observable near the wall and in the downstream part of the separation bubble. Finally, in Figs. 21 and 22 we show spanwise vorticity variations on selected lines in x and y directions, respectively. Note that the spanwise vorticity variations on the constant lines $x=0.45$ and 0.50 (shown in Fig. 22) represent one of the highest reconstruction errors, as re-

TABLE III. The rms error for DNS data reconstruction.

Gappy DNS data Equidistant grid points	rms error
10×10	0.702
20×20	0.356
30×30	0.206

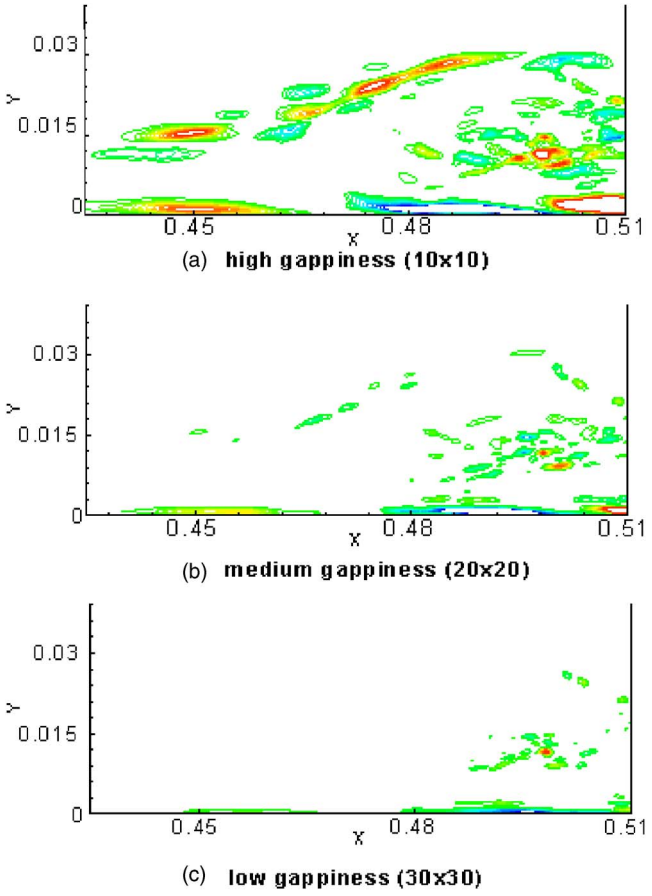

FIG. 20. Distribution of reconstruction error in the computational domain for different ratios of gappy DNS data (21 contour levels are shown; [−6:6]).

vealed in Fig. 20. It is seen that except for very large gappy data, Kriging interpolation can be faithfully used to enhance the data.

C. Kriging interpolation of three-dimensional PIV data

Even though PIV techniques are rapidly developing for three-dimensional experimental measurements, the resolution in certain directions may still not be sufficient for modern data visualization methods (e.g., see Jeong and Hussain[28] for the λ_2 method), so accurate interpolation/enhancement in certain direction(s) is necessary in order to implement these methods. In this section, we interpolate full *three-dimensional* stereoscopic PIV measurements carried out by Lang[16] for a flat plate with separation bubble. While his three-dimensional measurements in streamwise (x) and spanwise (z) directions are quite finely sampled (81 points in x and 44 points in z direction), only nine equidistant planes ($y=4,6,8,\ldots,20$) are available for the wall-normal direction. Therefore, our task is to employ Kriging interpolation to increase the resolution in the wall-normal direction. Since the no-slip condition requires that the velocity vector be zero on the wall, we incorporate this information into our Kriging interpolation in addition to the given nine wall-normal planes. The resolution of 3D PIV data can be enhanced by employing Kriging interpolation on each $x=$const plane or on a 3D zone. First, we performed Kriging interpolation separately on each $x=$const plane. We also performed Kriging interpolation on a three-dimensional domain (not individual planes). For this case, however, the computational domain needed to be partitioned into subdomains (64 volumes) in order to be able to compute the correlation matrix with regard to the available computer resources and efficiency. It is found out that both two- and three-dimensional application of Kriging interpolation have been in good agreement with each other. We performed Kriging interpolation for all 18 phase-averaged snapshots available from 3D PIV measurements. Here, we present results for enhancement of a representative snapshot. Figures 23–25 show instantaneous stereo-PIV data (top figure) of Lang[16] and corresponding enhancement with Kriging interpolation (bottom figure). Figure 23 illustrates the velocity vectors at a selected plane $x=360$, while Figs. 24 and 25 show velocity vectors at the peak ($z=120$) and valley ($z=135$) planes, respectively. Figure 26 shows the velocity vectors of selected "new" (unknown) planes ($y=5$, 11, and 15) calculated by Kriging interpolation.

VI. CONCLUSIONS

In this paper, POD and Kriging methods are investigated for the purpose of data reconstruction and spatial enhancement (e.g., interpolation to high-resolution and/or smoothing

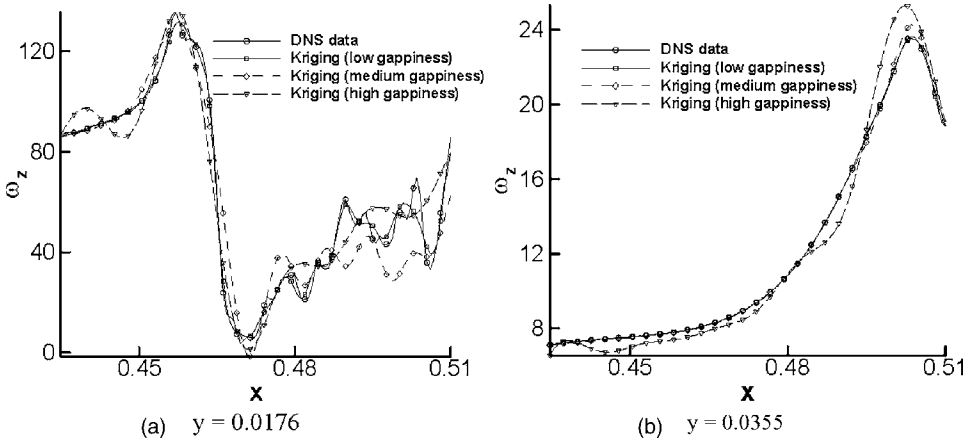

FIG. 21. Reconstruction of spanwise vorticity variation in the x direction using Kriging interpolation.

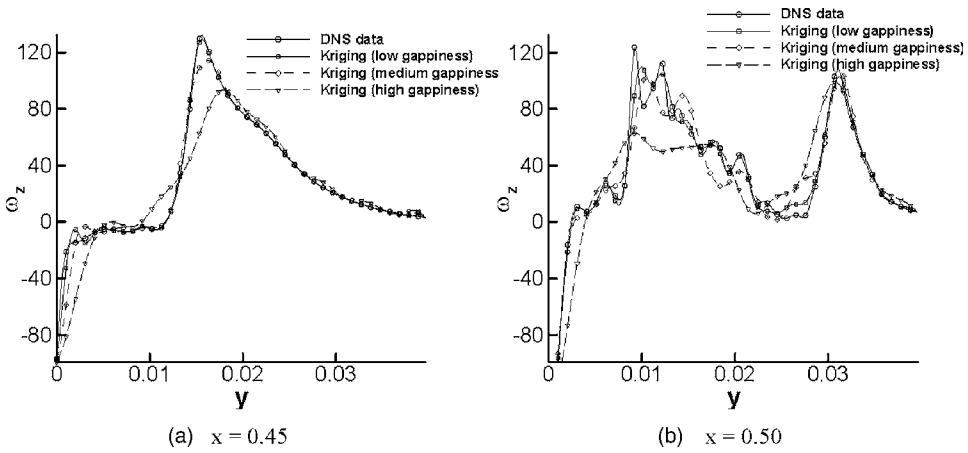

FIG. 22. Reconstruction of spanwise vorticity variation in the y direction using Kriging interpolation.

of noisy data) of experimental data for a transitional boundary layer with a laminar separation bubble. For the first procedure, POD is applied to DNS data to extract the DNS-based POD modes, which are then projected onto available experimental data in order to obtain the coefficients of the *hybrid* model based on the DNS modes. The hybrid model is then used to enhance (interpolate and smooth) the experimental data as well as for "extrapolation" since the model coefficients do not depend on spatial variation. In fact, we showed that near-wall spanwise vorticity, which is not available from experimental data, can be recovered faithfully.

We have also shown that Kriging interpolation can be used effectively for the reconstruction, interpolation, and smoothing of *two*- and *three*-dimensional experimental data. Comparing POD-based and Kriging interpolation, it is found out that for very low resolution of experimental data, DNS-based interpolation (if available) is superior over Kriging interpolation. On the other hand, Kriging interpolation works well for sufficiently high-resolution experimental/numerical data. Both procedures effectively eliminate the background noise and measurement errors in experimental data. Unlike the DNS-based procedure, the performance of the Kriging procedure drops sharply when it is used for extrapolation, therefore its usage should practically be limited solely for interpolation. We have shown that PIV-based POD modes are noisy, and by smoothing these modes by Kriging interpolation, noise-free reconstruction of PIV data can be achieved. Then, the coefficients can also be interpolated by

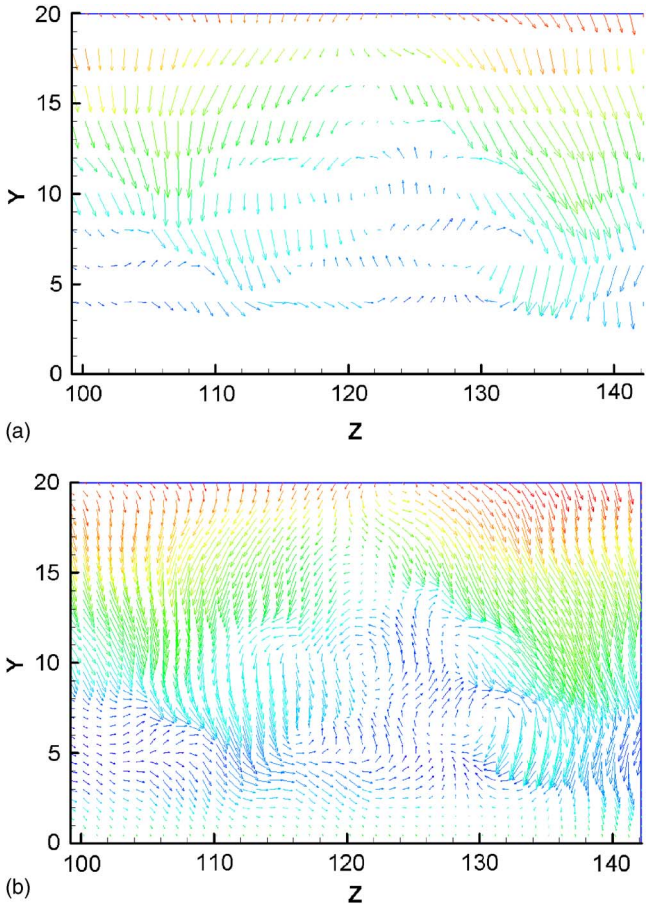

FIG. 23. Enhancement of 3D stereo-PIV data by Kriging interpolation (velocity vectors at plane $x=360$). (a) Instantaneous PIV data ($44\times\mathbf{10}$), (b) Kriging interpolation ($44\times\mathbf{81}$).

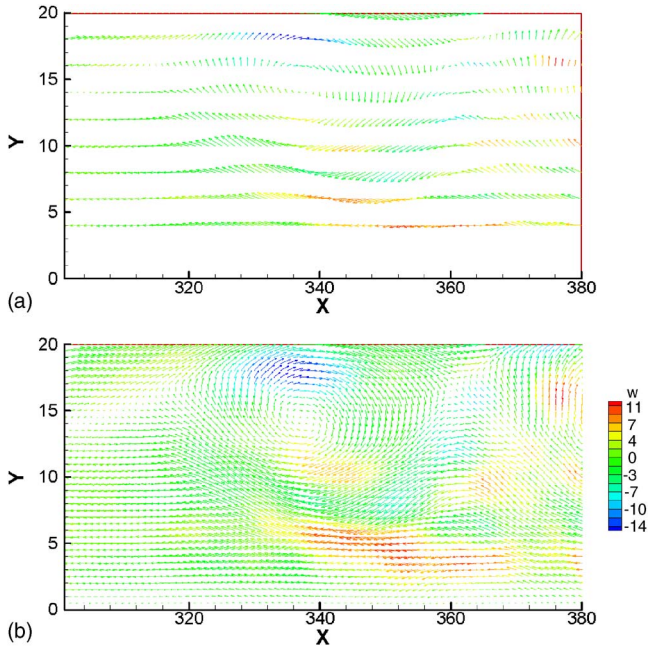

FIG. 24. Enhancement of 3D stereo-PIV data by Kriging interpolation (velocity vectors at peak plane $z=120$). (a) Instantaneous PIV data ($44\times\mathbf{10}$), (b) Kriging interpolation ($44\times\mathbf{81}$).

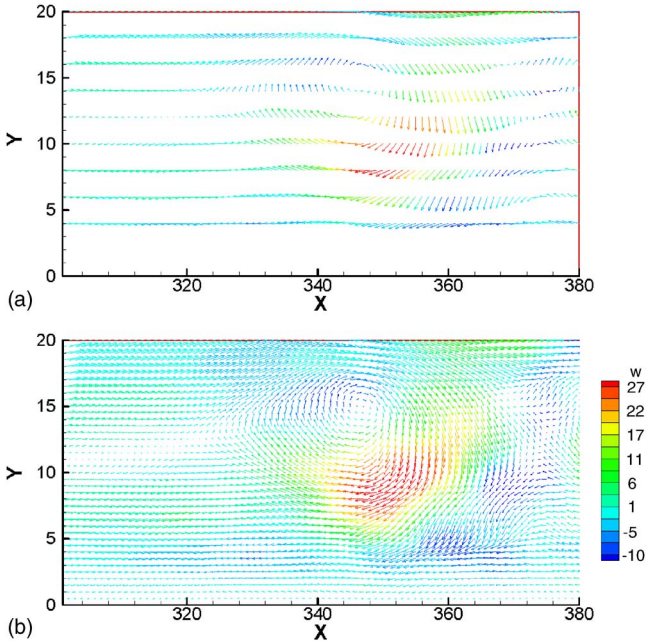

FIG. 25. Enhancement of 3D stereo-PIV data by Kriging interpolation (velocity vectors at valley plane $z=130$). (a) Instantaneous PIV data ($44\times\mathbf{10}$), (b) Kriging interpolation ($44\times\mathbf{81}$).

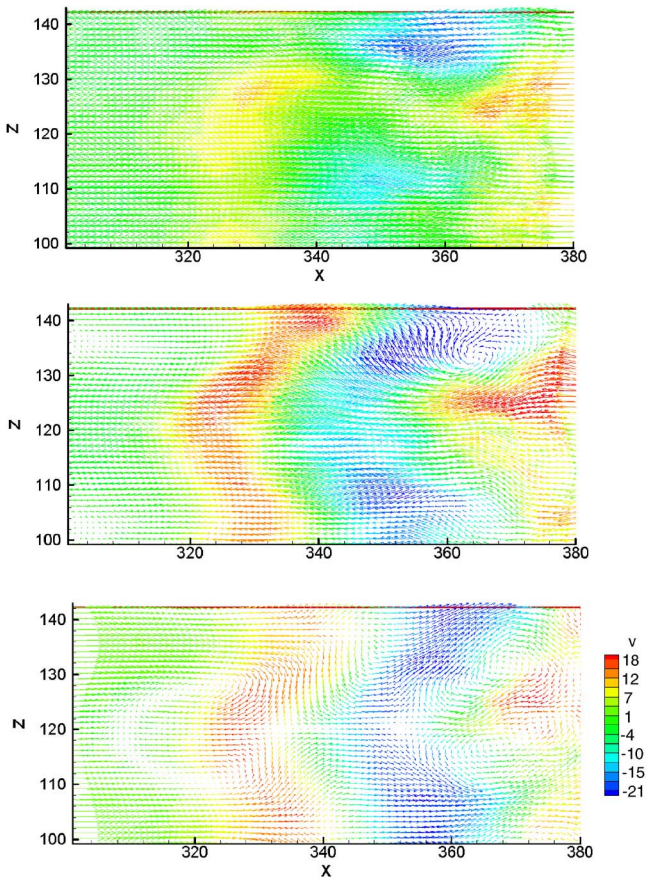

FIG. 26. The velocity vectors of new (unknown) planes estimated by Kriging interpolation. From top to bottom: $y=5$, 11, and 15.

piecewise cubic Hermite interpolating polynomials to increase both spatial and temporal resolution of the PIV data.

In general, it is important to note that in Kriging interpolation, the correlation function and the corresponding correlation parameter are suitably selected so that the correlation model predicts the design datasets almost exactly. However, when the values of the design dataset are not exact, i.e., if the source points have some uncertainty or contain background noise as in experimental data, the Gaussian correlation function with an appropriate correlation parameter should be used to obtain smoother interpolated data. It has been shown that the degree of smoothness can be controlled by the correlation parameter. On the other hand, when the design data sets are exact (i.e., free from noise and background disturbances as in DNS), Kriging interpolation based on the exponential, spline, or Gauss function (with large correlation parameters) can be used.

For future work, the following issues might be interesting to investigate: (i) the DNS-based procedure can be utilized to predict large missing regions and compare with Kriging predictions, (ii) a hybrid spatio-temporal dataset can be formed by combining the experimental and numerical snapshots in a certain way (e.g., consecutively) so that data reconstruction and enhancement procedures investigated in this paper are performed utilizing the *hybrid* POD modes, (iii) currently there is no guarantee that the reconstructed flow in the missing region satisfies the conservation equations of the flow. However, in a future work, it may be possible to implement a Kriging interpolation in an iterative scheme such that, for example, the recovered missing region satisfies the continuity equation.

ACKNOWLEDGMENTS

One of the authors (H.G.) gratefully acknowledges the financial support of the Deutsche Forschungsgemeinschaft (DFG) for his visit to IAG, Universität Stuttgart, which made the present work possible. The authors would like to thank Dr. M. Lang and Dr. O. Marxen for providing their latest stereo-PIV and DNS data sets, respectively. This research is supported by DFG SPP 1147 "Bildgebende Messverfahren für die Strömungsanalyse" as well as TÜBİTAK and Julich Research Center.

[1] M. Linnick and U. Rist, "Vortex identification and extraction in a boundary-layer flow," in *Vision, Modeling, and Visualization Proceedings, November 16–18, Erlangen, Germany*, edited by G. Greiner, J. Hornegger, H. Niemann, and M. Stamminger (Akad. Verlagsges. Aka, Berlin, 2005), pp. 9–16.

[2] H. Gunes and U. Rist, "Proper orthogonal decomposition reconstruction of a transitional boundary layer with and without control," Phys. Fluids **16**, 2763 (2004).

[3] R. D. Prabhu, S. S. Collis, and Y. Chang, "The influence of control on proper orthogonal decomposition of wall-bounded turbulent flows," Phys. Fluids **13**, 520 (2001).

[4] S. Sirisup, G. E. Karniadakis, Y. Yang, and D. Rockwell, "Wave-structure interaction simulation driven by quantitative imaging," Proc. R. Soc. London, Ser. A **460**, 729 (2004).

[5] X. Ma, G. E. Karniadakis, H. Park, and M. Gharib, "DPIV-driven flow simulation: A new computational paradigm," Proc. R. Soc. London, Ser. A **459**, 547 (2003).

[6] J. C. Davis, *Statistics and Data Analysis in Geology*, 3rd ed. (John Wiley, New York, 2002).

[7]M. Stein, *Interpolation of Spatial Data: Some Theory for Kriging* (Springer-Verlag, Berlin, 1999).
[8]E. H. Isaaks and R. M. Srivastava, *Introduction to Applied Geostatics* (Oxford University Press, New York, 1989).
[9]J. Sacks, W. J. Welch, T. J. Mitchell, and H. P. Wynn, "Design and analysis of computer experiments," Stat. Sci. **4**, 409 (1989).
[10]S. Lophaven, H. Nielsen, and J. Sondergaard, "DACE—A Matlab Kriging Toolbox, Version 2.0," Report No. IMM-REP-2002-12, Informatics and Mathematical Modelling, DTU (2002).
[11]S. Lophaven, H. Nielsen, and J. Sondergaard, "Aspects of the Matlab Toolbox DACE," Report No. IMM-REP-2002-13, Informatics and Mathematical Modelling, DTU (2002).
[12]H. B. Nielsen and K. F. Thuesen, "Surrogate models," Sixth Workshop of the European Research Consortium on Informatics and Mathematics (ERCIM) Work Group on Matrix Computations and Statistics, Copenhagen, Denmark, 1–3 April 2005.
[13]H. Gunes, S. Sirisup, and G. E. Karniadakis, "Gappy data: To Krig or not to Krig?" J. Chem. Phys. **212**, 358 (2006).
[14]H. E. Cekli and H. Gunes, "Spatial resolution enhancement and reconstruction of mixed convection data using the Kriging method," in Proceedings of ASME International Mechanical Engineering Congress and Exposition, Chicago, 5–10 November 2006.
[15]D. Venturi and G. E. Karniadakis, "Gappy data and reconstruction procedures for flow past a cylinder," J. Fluid Mech. **519**, 315 (2004).
[16]M. Lang, "Experimentelle Untersuchungen zur Transition in einer laminaren Ablöseblase mit Hilfe der LDA und der PIV," dissertation, Universität Stuttgart (2005).
[17]O. Marxen, "Numerical studies of physical effects related to the controlled transition process in laminar separation bubbles," dissertation, Universität Stuttgart (2005).
[18]M. Lang, U. Rist, and S. Wagner, "Investigations on controlled transition development in a laminar separation bubble by means of LDA and PIV," Exp. Fluids **36**, 43 (2004).
[19]O. Marxen and U. Rist, "Direct numerical simulation of non-linear transitional stages in an experimentally investigated laminar separation bubble," in *High Performance Computing in Science and Engineering '05*, edited by W. Nagel, W. Jäger, and M. Resch (Springer, Berlin, 2005), pp. 103–117.
[20]L. Sirovich, "Turbulence and the dynamics of coherent structures," Q. Appl. Math. **45**, 561 (1987).
[21]P. Holmes, J. L. Lumley, and G. Berkooz, *Turbulence, Coherent Structures, Dynamical Systems and Symmetry* (Cambridge University Press, Cambridge, 1996).
[22]A. E. Deane, I. G. Kevrekidis, G. E. Karniadakis, and S. A. Orszag, "Low-dimensional models for complex geometry flows: Application to grooved channels and circular cylinders," Phys. Fluids A **3**, 2337 (1991).
[23]B. Noack and H. Eckelman, "A low-dimensional Galerkin method for the three-dimensional flow around a circular cylinder," Phys. Fluids **6**, 124 (1994).
[24]D. Rempfer, "Investigations of boundary layer transition via Galerkin projections on empirical eigenfunctions," Phys. Fluids **8**, 175 (1996).
[25]A. Liakopoulos, P. A. Blythe, and H. Gunes, "A reduced dynamical model of convective flows in tall laterally heated cavities," Proc. R. Soc. London, Ser. A **453**, 663 (1997).
[26]C. Jing, D. Henry, H. B. Hadid, and N. Imaishi, "Low-order dynamical model for low-Prandtl number fluid flow in a laterally heated cavity," Phys. Fluids **15**, 2152 (2003).
[27]X. Ma and G. E. Karniadakis, "A low-dimensional model for simulation three-dimensional cylinder flow," J. Fluid Mech. **458**, 181 (2002).
[28]J. Jeong and F. Hussain, "On the identification of a vortex," J. Fluid Mech. **285**, 69 (1995).